[8] B. Sheleg and B. E. Spielman, "Broad band directional couplers using microstrip with dielectric overlays," *IEEE Trans. Microwave Theory Tech.*, vol. MTT-22, pp. 1216–1220, Dec. 1974.
[9] M. V. Schneider, "Microstrip lines for microwave integrated circuits," *BSTJ*, vol. 48, no. 5, pp. 1421–1444, May–June 1969.
[10] C. D. Hodgman, Ed., *Handbook of Chemistry and Physics*. Cleveland, OH: Chemical Rubber Publishing Co., 1961, p. 2628.
[11] T. L. Simpson and B. Tseng, "Dielectric loss in microstrip lines," *IEEE Trans. Microwave Theory Tech.*, vol. MTT-24, pp. 106–108, Feb. 1976.
[12] M. V. Schneider, "Dielectric loss in integrated microwave circuits," *BSTJ*, vol. 48, pp. 2325–2332, Sept. 1969.
[13] R. A. Pucel, D. J. Masse, and C. P. Hartwig, "Losses in microstrip," *IEEE Trans. Microwave Theory Tech.*, vol. MTT-16, pp. 342–350, June 1968.
[14] A. Gopinath, R. Horton, and B. Easter, "Microstrip loss calculations," *Electron. Letts.*, vol. 6, no. 2, pp. 40–41, Jan. 22, 1970.
[15] J. McDade and D. Stockman, "Microwave integrated circuit techniques," AFAL/TEM, Wright Patterson AFB, OH, Tech. Rep. AFAL-TR-73-234, May 1973.

Analysis of Distributed-Lumped Strip Transmission Lines

TADAHIKO SUGIURA

Abstract—**A calculation method for obtaining characteristic impedances and phase velocities of striplines, which are regarded as consisting of distributed-lumped elements such as so-called wiggly lines, is presented with numerical results. The numerical calculations have been carried out for a) single stripline with slots at the outer edges, b) coupled stripline with rectangular wiggling, and c) coupled stripline with slots at the outer edges. Experimental work has also been accomplished to verify the present method. Results show good agreement with calculations.**

I. Introduction

RECENTLY, stripline circuits have become widely used at microwave frequencies, in accordance with microwave integrated circuit developments. Parallel coupled striplines are especially useful for realizing filters, directional couplers, and other microwave circuits.

In an ordinary coupled line, shown in Fig. 1(a), the phase velocities of the even and odd modes differ because of the inhomogeneity of the ambient medium. The difference in the two velocities usually causes undesired degradation of the circuits. Podell has solved this problem by introducing the wiggling technique [1]; that is, wiggling the coupled edges as shown in Fig. 1(b). Due to the different distributions of the even and odd mode currents, it is possible to raise the odd mode inductance more than the even mode inductance by the wiggling technique. Generalizing this idea, deRonde has shown that a tightly coupled line can be realized by slotting the outer edges of the wiggly line, as shown in Fig. 1(c) [2]. These lines can be regarded as consisting of distributed-lumped elements. The inductance or the capacitance of a stripline may be widely varied by applying the above-mentioned distributed-lumped technique.

For practical applications, however, tedious cut-and-try experiments are needed to obtain the desired value, because available experimental data are very scarce and no quantitative analysis has been reported for these lines. This paper presents a calculation method to obtain the characteristic impedance and the phase velocity of the distributed-lumped striplines. Numerical results obtained with the aid of a digital computer are compared with experimental data.

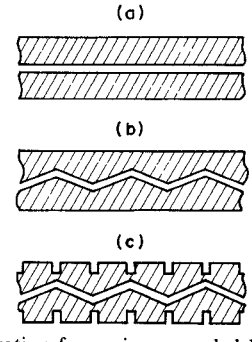

Fig. 1. Strip configuration for various coupled lines: (a) ordinary line, (b) and (c) distributed-lumped lines.

II. Theory

A. General Considerations

The distributed-lumped stripline has a periodic structure, as shown in Fig. 2. On the assumption that one unit section of the periodic structure is much shorter than the wavelength, static theory can be applied for determining the inductance and the capacitance per unit section, because the voltage and the current are regarded as constant over the unit section. If the inductance and the capacitance are obtained, the characteristic impedance and the phase velocity are readily calculated, according to ordinary transmission line theory. Accordingly, the problem is reduced to calculations of the inductance and the capacitance per unit section.

Although various types of line structure can be considered in distributed-lumped lines, the calculation model chosen is

Manuscript received August 15, 1973; revised January 21, 1977.
The author is with the Central Research Laboratories, Nippon Electric Company, Ltd., Kawasaki 213, Japan.

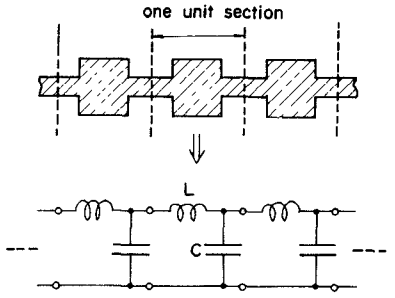

Fig. 2. Periodic structure in distributed-lumped line and its equivalent circuit.

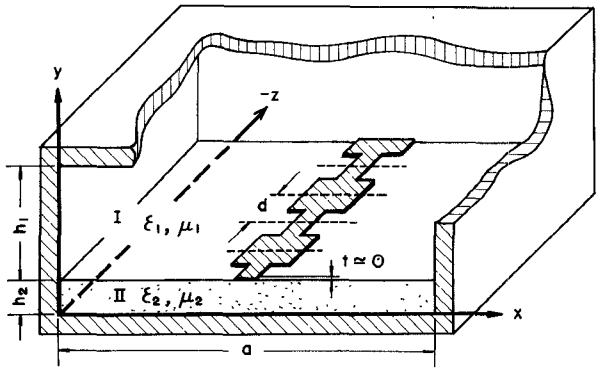

Fig. 3. Distributed-lumped stripline calculation model.

as shown in Fig. 3, where the following three restrictions are set to simplify the analysis. a) The line is a shielded microstrip with an infinitely thin strip conductor. b) The line is symmetrical about the x-y plane (therefore $z = kd$ planes, where k = integer, and d = length of a unit section). c) The strip configuration of a unit section can be partitioned into rectangles.

B. Capacitance Calculation

Letting ψ_{e1} and ψ_{e2} represent the electrostatic potentials in regions I and II in Fig. 3, respectively, ψ_{e1} and ψ_{e2} are given by

$$\psi_{e1} = \sum_{m=1}^{\infty}\sum_{n=0}^{\infty} A_{mn} \sin\frac{m\pi x}{a}\cos\frac{n\pi z}{d} \cdot \sinh k_{mn}(h_1 + h_2 - y) \tag{1a}$$

$$\psi_{e2} = \sum_{m=1}^{\infty}\sum_{n=0}^{\infty} B_{mn} \sin\frac{m\pi x}{a}\cos\frac{n\pi z}{d}\sinh k_{mn}y \tag{1b}$$

where

$$k_{mn} = \sqrt{\left(\frac{m\pi}{a}\right)^2 + \left(\frac{n\pi}{d}\right)^2}$$

and A_{mn} and B_{mn} are unknown coefficients. Since total electrostatic energy U_e, stored in the unit section, is given by $\frac{1}{2}\int_v \boldsymbol{E}\cdot\boldsymbol{D}\,dv$, substituting (1a) and (1b) into this expression gives

$$U_e = \frac{ad}{16}\sum_{m=1}^{\infty}\sum_{n=0}^{\infty} P(n)k_{mn} \cdot (\varepsilon_1 A_{mn}^2 \sinh 2k_{mn}h_1 + \varepsilon_2 B_{mn}^2 \sinh 2k_{mn}h_2) \tag{2}$$

where

$$P(n) = \begin{cases} 1 & (n \neq 0) \\ 2 & (n = 0). \end{cases}$$

In order to eliminate unknown coefficients A_{mn} and B_{mn}, the following boundary conditions at $y = h_2$ are used

$$\psi_{e1} = \psi_{e2} \tag{3a}$$

$$\varepsilon_2\frac{\partial\psi_{e2}}{\partial y} - \varepsilon_1\frac{\partial\psi_{e1}}{\partial y} = \rho_e(x,z) \tag{3b}$$

where ρ_e is the electric charge distribution at $y = h_2$. Therefore, $\rho_e = 0$, except on the strip conductor. By using (1a), (1b), (3a), and (3b), A_{mn} and B_{mn} can be expressed by ρ_e. The results are then substituted into (2). Total electrostatic energy U_e is now rewritten as

$$U_e = \frac{2}{ad}\sum_{m=1}^{\infty}\sum_{n=0}^{\infty} G_e(m,n) \cdot \left\{\int_0^d\int_0^a \rho_e(x,z)\sin\frac{m\pi x}{a}\cos\frac{n\pi z}{d}\,dx\,dz\right\}^2 \tag{4}$$

where

$$G_e(m,n) = \frac{1}{P(n)k_{mn}}(\varepsilon_1 \coth k_{mn}h_1 + \varepsilon_2 \coth k_{mn}h_2)^{-1}.$$

Capacitance per unit section is given by

$$C = \frac{Q}{V} = \frac{Q^2}{2U_e} \tag{5}$$

where Q is the total electric charge on the strip and given by

$$Q = \int_0^d\int_0^a \rho_e(x,z)\,dx\,dz. \tag{6}$$

Therefore, if unknown charge distribution ρ_e is obtained, capacitance is calculated from (4), (5), and (6).

C. Inductance Calculation

Calculation of the inductance can be made by the same procedure as that for calculating capacitance. For capacitance calculation, the whole region of the unit section has been divided into air and substrate layers, wherein the electrostatic potentials are individually determined. Since each layer is simply connected and has no current in it, the magnetostatic potentials, denoted by ψ_{m1} and ψ_{m2}, can also be defined [3] and calculated as follows:

$$\psi_{m1} = \sum_{m=1}^{\infty}\sum_{n=0}^{\infty} C_{mn}\cos\frac{m\pi x}{a}\cos\frac{n\pi z}{d}\cosh k_{mn}(h_1 + h_2 - y) \tag{7a}$$

$$\psi_{m2} = \sum_{m=1}^{\infty}\sum_{n=0}^{\infty} D_{mn}\cos\frac{m\pi x}{a}\cos\frac{n\pi z}{d}\cosh k_{mn}y \tag{7b}$$

where C_{mn} and D_{mn} are the unknown coefficients to be eliminated. Taking $H = -\psi_m$ into consideration, the total

magnetostatic energy U_m stored within the unit section is given by

$$U_m = \frac{ad}{16} \sum_{m=1}^{\infty} \sum_{n=0}^{\infty} P(n) k_{mn} \cdot (\mu_1 C_{mn}^2 \sinh 2k_{mn}h_1 + \mu_2 D_{mn}^2 \sinh 2k_{mn}h_2). \quad (8)$$

At the boundary between the air and the substrate layers, the normal component of the magnetic flux density is continuous. Thus, at $y = h_2$,

$$\mu_1 \frac{\partial \psi_{m1}}{\partial y} = \mu_2 \frac{\partial \psi_{m2}}{\partial y} \quad (9a)$$

$$\mu_1 \frac{\partial \psi_{m1}}{\partial y} = \rho_m(x,z) \quad (9b)$$

where ρ_m is the normal component of the magnetic flux density. This can be also recognized, in comparison to the electrostatic case, as magnetic charge distribution of a hypothetical magnetic dipole layer at $y = h_2$. Since the normal component of the magnetic flux density cannot exist on the conductor surface, $\rho_m = 0$ on the strip conductor. Unknown coefficients C_{mn} and D_{mn} can be eliminated from (8) by using (9a) and (9b)

$$U_m = \frac{2}{ad} \sum_{m=1}^{\infty} \sum_{n=0}^{\infty} G_m(m,n) \cdot \left\{ \int_0^d \int_0^a \rho_m(x,z) \cos \frac{m\pi x}{a} \cos \frac{n\pi z}{d} dx\, dz \right\}^2 \quad (10)$$

where

$$G_m(m,n) = \frac{1}{P(n)k_{mn}} \left(\frac{1}{\mu_1} \coth k_{mn}h_1 + \frac{1}{\mu_2} \coth k_{mn}h_2 \right).$$

Inductance per unit section is given by

$$L = \frac{\Phi}{I} = \frac{\Phi^2}{2U_m} \quad (11)$$

where Φ is the total magnetic flux interlinking the strip conductor. Since the magnetic flux across one side of the strip conductor is equal in magnitude and opposite in sign to that across the other side

$$\Phi = \int \int_{S'} \rho_m(x,z)\, dx\, dz \quad (12)$$

where region S' is one side of the strip conductor at $y = h_2$.

D. Charge Distribution Determination

Charge distributions ρ_e and ρ_m are still unknown. An approximate charge distribution, however, can be determined by Rayleigh–Ritz's procedure [4]. Although actual charge distribution may be very complex, the approximate charge distribution will give good results, since the variational principle is utilized [5].

In the case of capacitance calculation, electric charge distribution is expressed in terms of known basis functions f_k as follows:

$$\rho_e(x,z) = \sum_{k=1}^{K} \alpha_k f_k(x,z) \quad (13)$$

where α_k are unknown coefficients that must be determined. Thomson's theorem states that, under the condition of total charge being constant, the charges residing on conductors will distribute themselves in such a way that the energy is minimized [5]. Thus the functional to be minimized is given by

$$F = U_e + \lambda(Q - 1) \quad (14)$$

where λ is the Lagrangian multiplier and condition $Q = 1$ is set to simplify (5) (capacitance calculation). In order to minimize F with respect to each α_k and λ, all partial derivatives $\partial F/\partial \alpha_k$ and $\partial F/\partial \lambda$ are set equal to zero. As a result, the following set of $K + 1$ inhomogeneous linear equations is obtained

$$\begin{bmatrix} A_{11} \\ \vdots \\ A_{K1} \\ B_1 \end{bmatrix} \cdots \begin{bmatrix} A_{1K} & B_1 & \alpha_1 \\ \vdots & \vdots & \vdots \\ A_{KK} & B_K & \alpha_K \\ B_K & 0 & \lambda \end{bmatrix} = \begin{bmatrix} 0 \\ \vdots \\ 0 \\ 1 \end{bmatrix} \quad (15)$$

where

$$A_{kl} = \frac{4}{ad} \sum_{m=1}^{\infty} \sum_{n=0}^{\infty} G_e(m,n) \cdot \left\{ \int_0^d \int_0^a f_k(x,z) \sin \frac{m\pi x}{a} \cos \frac{n\pi z}{d} dx\, dz \right\} \cdot \left\{ \int_0^d \int_0^a f_l(x,z) \sin \frac{m\pi x}{a} \cos \frac{n\pi z}{d} dx\, dz \right\} \quad (16a)$$

$$B_k = \int_0^d \int_0^a f_k(x,z)\, dx\, dz. \quad (16b)$$

Thus the approximate charge distribution is determined by solving the linear equations for α_k and λ with the aid of a digital computer.

Accuracy is improved by increasing the number of basis functions and by solving a larger size matrix. If the number of basis functions is fixed, accuracy depends on how well the basis functions are able to approximate the actual charge distribution. Therefore, the choice of basis functions is important, from the standpoint of calculation efficiency.

In practical calculations, basis functions are chosen in the following manner. The whole region on a strip conductor is appropriately partitioned into rectangular subregions, as shown in Fig. 4. In each subregion, the charge distribution is independently expanded in a power series with respect to x and z. For example, in the case of Fig. 4, the charge distribution is expressed as

$$\rho_e(x,z) = \sum_{l=1}^{2} \rho_{el}(x,z) \quad (17a)$$

$$\rho_{el}(x,z) = \begin{cases} \sum_{i=1}^{I} \sum_{j=1}^{J} \alpha_{ij} x^{i-1} z^{j-1} & \text{(on subregion } l\text{)} \\ 0 \quad \text{(otherwise).} \end{cases} \quad (17b)$$

Since the term number of the power series is independently selected in each subregion, it is possible to remove the unnecessary higher terms for a subregion, where the charge distribution varies slowly and can be expressed without higher terms.

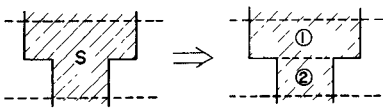

Fig. 4. Region S partitioned into two subregions.

Due to this choice of basis functions, the double integral in (16a) is reduced to the product of two single integrals of the following form:

$$\int x^{i-1} \sin \frac{m\pi x}{a} dx \int z^{j-1} \cos \frac{n\pi z}{d} dz.$$

This can be easily calculated in analytic form. Moreover, the above integral decays as fast as $(mn)^{-1}$ for large m and n; therefore, the double summation in (16a) decays as fast as $(m^2n^2\sqrt{m^2+n^2})^{-1}$. Thus the matrix elements in (15) are obtained after truncating at some finite term numbers M and N.

For the inductance calculation, the approximate magnetic charge can also be determined in the same manner.

III. Numerical Results

A. Single Stripline with Slots at Outer Edges

For practical applications, the distributed-lumped line with a single strip conductor is not as important as that with coupled conductors, but experimental work on the former is much easier than that on the latter, because the single stripline has only one fundamental mode. Therefore, the calculation has been carried out in order to compare calculated results with measured results. The calculated line physical structure is shown in Fig. 5(a), where the relative dielectric constant of ten, three in the alumina substrate, has been determined by the measurement described in [7]. Because of the symmetry, calculation has been carried out for only one half side of the line. The previously described subregions are also shown in Fig. 5(a).

To examine the accuracy, the capacitance values for increasing the number of basis functions have been calculated. Since the strip conductor is partitioned into two subregions, and the term numbers of the power series in the two subregions are chosen to be equal, the matrix size becomes $2IJ + 1$. The result is shown in Fig. 6. The calculated capacitance becomes larger when increasing the term number of the power series, because the variational principle is utilized [7]. However, for a large number of the power series, the increase in capacitance is much smaller than that for a small number. For example, the capacitance increases 5.46 percent when increasing the term numbers from $I = J = 1$ to $I = J = 2$, 1.51 percent from $I = J = 2$ to $I = J = 3$, and 0.54 percent from $I = J = 3$ to $I = J = 4$. Therefore, term numbers I and J are set equal to three for capacitance calculation, considering calculation efficiency. The accuracy, in this case, may be estimated within a few percent.

For inductance calculation, the whole region where the magnetic charge exists is partitioned into three subregions, as shown in Fig. 5(a). In subregions 2 and 3, term numbers I and J are also set equal to three. In subregion 1, I is set equal to three, but J is set equal to one. This implies that the variation in the z direction is neglected, because the actual magnetic charge in subregion 1 probably distributes almost uniformly in the z direction. The matrix size in this case becomes 22. These calculating conditions are summarized in Table I.

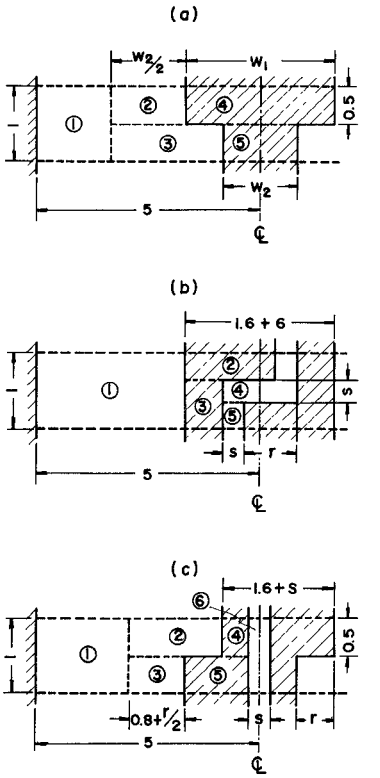

Fig. 5. Calculated distributed-lumped stripline ($h_1 = 5$, $h_2 = 1$, $\varepsilon_{r2} = 10.3$, and $\varepsilon_{r1} = \mu_{r1} = \mu_{r2} = 1$): (a) single stripline with slots at outer edges, (b) coupled stripline with rectangular wiggling, and (c) coupled stripline with slots at outer edges.

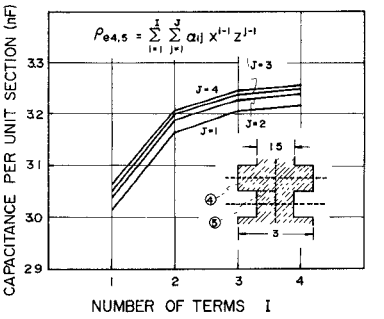

Fig. 6. Calculated capacitance when increasing power series term number.

The calculated results for the characteristic impedance are shown in Fig. 7 with experimental results, obtained by using a time-domain reflectometer. Fig. 7 shows that the measured impedances are somewhat higher, but their variation tendency shows good agreement with the calculated one. The left-end part of each solid line in Fig. 7 shows the calculated result for the $w_1 = w_2$ stripline or the uniform line. That value is coincident with the result calculated by applying a two-dimensional model [8]. Therefore, it can be recognized that differences between calculated and measured im-

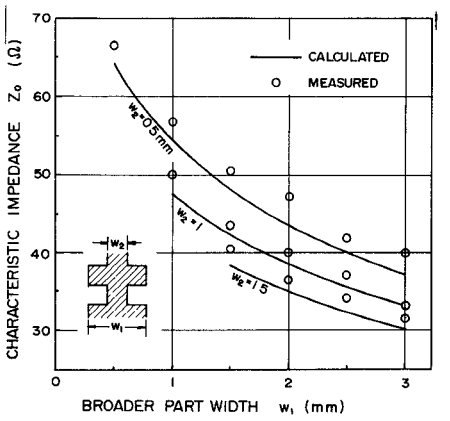

Fig. 7. Characteristic impedance of single stripline with slots at outer edges.

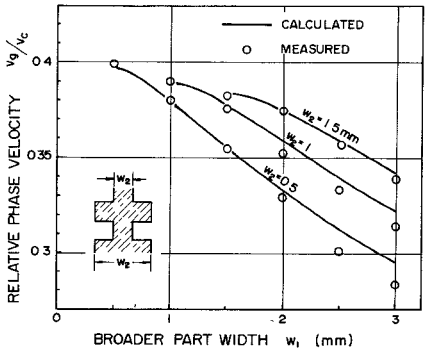

Fig. 8. Relative phase velocity of single stripline with slots at outer edges.

TABLE I
CALCULATING CONDITIONS FOR SINGLE STRIPLINE WITH SLOTS AT OUTER EDGES

	region	I	J
Magnetic charge	1	3	1
	2	3	3
	3	3	3
Electric charge	4	3	3
	5	3	3
Field	M=200, N=19		
Computation time	3 min./structure		

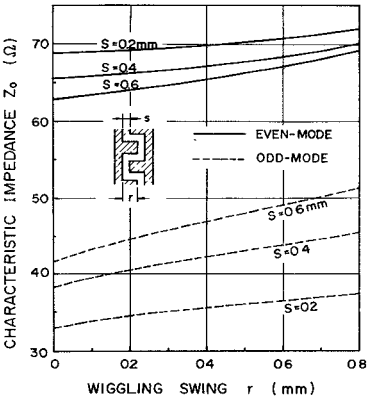

Fig. 9. Characteristic impedance of coupled stripline with rectangular wiggling.

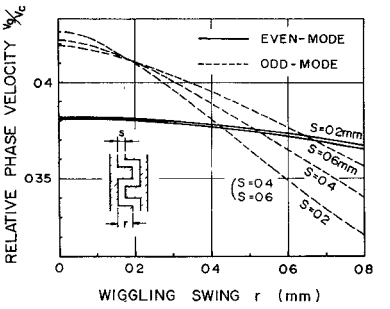

Fig. 10. Relative phase velocity of coupled stripline with rectangular wiggling.

TABLE II
CALCULATING CONDITIONS FOR COUPLED STRIPLINE WITH RECTANGULAR WIGGLING

	region	I	J
Magnetic charge	1	6	1
	4	3	3
	5	3	3
Electric charge	2	3	3
	3	3	3
Field	M=300, N=29		
Computation time	15 min./structure		

pedances are mainly caused by measuring inaccuracies encountered in the experiment.

The result for the relative phase velocity is shown in Fig. 8. The experiment in this case has been accomplished by measuring the guide wavelength at 2.0 GHz by the slotted line method. Calculated results in Fig. 8 show good agreement with the measured results, excepting that the measured values are slightly lower when the difference between w_1 and w_2 is relatively large.

B. Coupled Stripline with Rectangular Wiggling

Although only single striplines were treated in the previously described analysis, it can be also applied for coupled lines by using the matrix forms of the capacitance and inductance [10]. The ordinary wiggly line, which is now extensively used for the directional coupler, has a triangular strip configuration, as shown in Fig. 1(b). The calculation for such a line, however, is very complex, because the double integrals in (16a and b) cannot be reduced to single integrals. Thus the rectangular wiggly line shown in Fig. 5(b) has been chosen as an example. The calculation in this case was also carried out for only half of the line, because the strip configuration has odd symmetry. The calculating conditions, such as the term numbers of power series in the subregions, are summarized in Table II.

The results are shown in Figs. 9 and 10. Fig. 10 shows that the decrease in odd mode velocity, when increasing the wiggling swing, is much steeper than that of the even mode one, and that both mode velocities can be coincided by suitable choice of the wiggling swing. It also shows that the tighter the coupling, the steeper the decrease in the odd mode velocity. Taking the current distribution of each mode into consideration, these results are quite reasonable.

TABLE III
CALCULATING CONDITIONS FOR COUPLED STRIPLINE WITH SLOTS AT OUTER EDGES

	region	I	J
Magnetic charge	1	3	1
	2	3	3
	3	3	3
	6	3	1
Electric charge	4	3	3
	5	3	3
Field	M=300, N=19		
Computation time	10 min./structure		

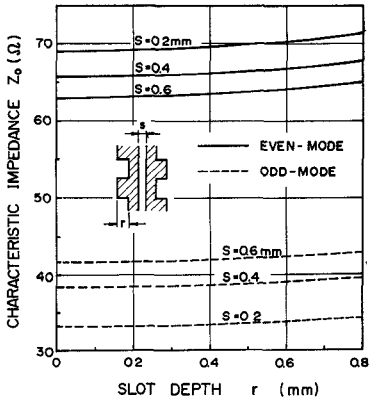

Fig. 11. Characteristic impedance of coupled stripline with slots at outer edges.

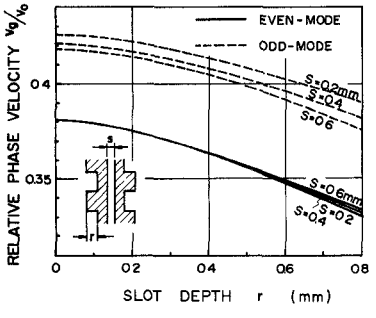

Fig. 12. Relative phase velocity of coupled stripline with slots at outer edges.

On the other hand, Fig. 9 shows that the characteristic impedance increases with increases in the wiggling swing. Therefore, it is concluded that the decrease in the phase velocity is mainly due to raising the inductance, rather than raising the capacitance.

C. Coupled Stripline with Slots at Outer Edges

Calculated results for the coupled line with slots at the outer edges, as shown in Fig. 5(c), are presented. In this type of line, conversely to the wiggly line, the differences of both the characteristic impedance and the phase velocity between two modes are considered to be increased, because of the raising effect of the even mode inductance. Therefore, tightly coupled lines or lines with a large difference in mode velocities, which are also utilized in directional couplers [9], may be realized.

The calculating conditions are summarized in Table III. The results for the characteristic impedance and the relative phase velocity are shown in Figs. 11 and 12, respectively. The result in Fig. 11 shows that the impedance difference between two modes is certainly increased, but this increase is much slighter than expected. Also, in Fig. 12, the increase in velocity difference is unrecognizably slight. These results imply that the current distribution on the outer edges of the strips is still relatively large, even in the odd mode. Therefore, narrower slots are necessary to effectively raise the even mode inductance.

IV. CONCLUSIONS

An analysis of the calculation of the characteristic impedances and the phase velocities of the distributed-lumped striplines has been described with numerical results. The analysis is based on static theory, on the assumption that the one unit section of the line is much shorter than the wavelength. The present method is novel, in that the capacitance and inductance can be calculated by using the same procedure.

Numerical calculations have been carried out for a) single stripline with slots at the outer edges, b) coupled stripline with rectangular wiggling, and c) coupled stripline with slots at the outer edges. In order to verify the present method, experimental work also has been accomplished for case a) lines. Results show good agreement with calculations.

For numerical calculations, a digital computer, NEAC-2200 model 500 (NEC), was used.

ACKNOWLEDGMENT

The author wishes to thank E. Kataoka for his assistance in the experiments and Miss R. Kobayashi for her computational assistance. He also wishes to thank Dr. K. Ayaki, Dr. H. Kaneko, Dr. M. Sugiyama, and Dr. H. Katoh for their encouragement and guidance.

REFERENCES

[1] A. Podell, "A high directivity microstrip coupler technique," in *1970 G-MTT Symposium Digest*, pp. 33–36.
[2] F. C. DeRonde, "Recent developments in broadband directional couplers on microstrip," in *1972 G-MTT Symposium Digest*, pp. 215–217.
[3] J. A. Stratton, *Electromagnetic Theory*. New York: McGraw-Hill, 1941, chap. 4.
[4] R. Courant and D. Hilbert, *Methoden der Mathematischen Physik*. Verlag von Julius Springer, 1931, chap. 4.
[5] M. Maeda, "An analysis of gap in microstrip transmission lines," *IEEE Trans. Microwave Theory Tech.*, vol. MTT-20, pp. 390–396, June 1972.
[6] R. E. Collin, *Field Theory of Guided Waves*. New York: McGraw-Hill, 1960, chap. 1.
[7] J. Q. Howell, "A quick accurate method to measure the dielectric constant of microwave integrated-circuit substrates," *IEEE Trans. Microwave Theory Tech.*, vol. MTT-21, pp. 142–143, Mar. 1973.
[8] D. L. Gish and O. Graham, "Characteristic impedance and phase velocity of a dielectric-supported air strip transmission line with side walls," *IEEE Trans. Microwave Theory Tech.*, vol. MTT-18, pp. 131–148, Mar. 1970.
[9] J. E. Dalley, "A strip-line directional coupler utilizing a nonhomogeneous dielectric medium," *IEEE Trans. Microwave Theory Tech.*, vol. MTT-17, pp. 706–712, Sept. 1969.
[10] D. W. Kammler, "Calculation of characteristic admittances and coupling coefficients for strip transmission lines," *IEEE Trans. Microwave Theory Tech.*, vol. MTT-16, pp. 925–937, Nov. 1968.